Int J Adv Manuf Technol (2004) 24: 794–805
DOI 10.1007/s00170-003-1797-5

ORIGINAL ARTICLE

X.-W. Liu · K. Cheng · D. Webb · A.P. Longstaff · M.H. Widiyarto

Improved dynamic cutting force model in peripheral milling. Part II: experimental verification and prediction

Received: 14 February 2003 / Accepted: 11 May 2003 / Published online: 19 May 2004

Abstract Cutting trials reveal that a measure of cutter run-out is always unavoidable in peripheral milling. This paper improves and extends the dynamic cutting force model of peripheral milling based on the theoretical analytical model presented in Part I [1], by taking into account the influence of the cutter run-out on the undeformed chip thickness. A set of slot milling tests with a single-fluted helical end-mill was carried out at different feed rates, while the 3D cutting force coefficients were calibrated using the averaged cutting forces. The measured and predicted cutting forces were compared using the experimentally identified force coefficients. The results indicate that the model provides a good prediction when the feed rate is limited to a specified interval, and the recorded cutting force curves give a different trend compared to other published results [8]. Subsequently, a series of peripheral milling tests with different helical end-mill were performed at different cutting parameters to validate the proposed dynamic cutting force model, and the cutting conditions were simulated and compared with the experimental results. The result demonstrates that only when the vibration between the cutter and workpiece is faint, the predicted and measured cutting forces are in good agreement.

Keywords 3D · Cutting force · Dynamic · Experiment · Peripheral milling · Prediction · Verification

Nomenclature

Ω	radial immersion angle
α_e	effective rake angle
α_{e0}	initial effective rake angle
α_n	normal rake angle
α_r	radial rake angle
β	helix angle of end mill, inclination angle of oblique cutting
θ	tool rotation angle
φ	helix lag angle
φ_s, φ_e	helix lag angular locations of the starting and ending points of contact
φ_{e0}	initial location angle of the cutter centre relative to spindle centre
φ_i	position angle of a point on the cutting edge of the ith helical flute
ψ	axial immersion angle of a tooth within b_a
ω	spindle rotation angle speed
δ_e	cutter run-out value
$\mathrm{d}F_{ti}$, $\mathrm{d}F_{ri}$, $\mathrm{d}F_{ai}$	differential cutting force components of the ith helical flute in tangential, radial and axial directions
$\mathrm{d}F_{ix}$, $\mathrm{d}F_{iy}$, $\mathrm{d}F_{iz}$	differential cutting force components of the ith helical flute in x, y and z directions
F_{ix}, F_{iy}, F_{iz}	total cutting force components of the ith helical flute in x, y and z directions
F_x, F_y, F_z	total cutting force components in x, y and z directions
K_s	tangential cutting force coefficient
R	tool radius
$R'_i(\varphi_i)$	actual cutting radius of the ith tooth in angle position φ_i
V	cutting speed
V_c	chip speed
b_a	axial depth of cut (peripheral milling)
c_1	radial cutting force ratio
c_2	axial cutting force ratio
d	radial depth of cut
f_t	feed per tooth per revolution
m	number of cutter flutes
n	spindle rotation speed (rpm)
t_{ime}	time
t	undeformed chip thickness

X.-W. Liu · K. Cheng (✉) · D. Webb
School of Engineering,
Leeds Metropolitan University,
City Campus, Leeds LS1 3HE, UK
E-mail: k.cheng@lmu.ac.uk

A.P. Longstaff · M.H. Widiyarto
Ultra Precision Engineering Centre,
University of Huddersfield,
Huddersfield, UK

$t_i(\varphi_i)$	undeformed chip thickness of the ith tooth in angle position φ_i
$\delta t_i(\varphi_i)$	variation of undeformed chip thickness caused by cutter run-out
t_0	initial undeformed chip thickness
t_c	chip thickness
u_0	initial total cutting energy per unit volume
SF	spindle frequency
TPF	tooth passing frequency

1 Introduction

An accurate dynamic cutting force model is essential for the precise prediction of tool and workpiece deflection as well as the control of vibrations in peripheral milling. Studies on theoretical modelling and experimental verification of dynamic cutting forces in peripheral milling have been investigated [2–8] and have been reviewed by Smith and Tlusty [9]. Very few researchers working on the cutting force models have focused their attention on the following experimental issues, i.e., the unavoidable cutter run-out and vibrations between the cutter and workpiece in the cutting process, as well as the successive inconsistency of measured cutting forces [10, 11]. Some researchers attempted to address the cutter run-out in their work [5–7], however, no attention was given to cutting force models, especially experimental verification of the models.

In the previous paper [1], a theoretical model with an analytical expression for the prediction of dynamic cutting forces in peripheral milling was presented. In the further experimental verification and application of the model, it is found that there should be a measurement of the cutter run-out, which significantly influences dynamic cutting forces. Considering the influence of the cutter run-out, this paper provides an improvement of the theoretical model. Furthermore, for the integration of the model, the axial cutting force component is formulated in the model as well. For the verification of the model, a series of well-designed cutting tests are carried out. For each cutting test, not only the dynamic cutting forces are recorded, the cutter run-out and the spindle and workpiece vibrations are measured as well.

2 Theoretical background

The details of the theoretical dynamic cutting force model for peripheral milling was presented in the previous paper [1], but the brief mathematical formulation related to this paper is summarised in this section. Figure 1a shows the geometric model of a helical end mill, which can be visualised as a combination of a number of slices along its z-direction. Within each slice, the cutting action for an individual tooth can be modelled as for single point oblique cutting, and the differential tangential, normal and axial cutting forces at any point on the rake face can be obtained from the oblique cutting model [1, 12, 13], as shown in Fig. 1b:

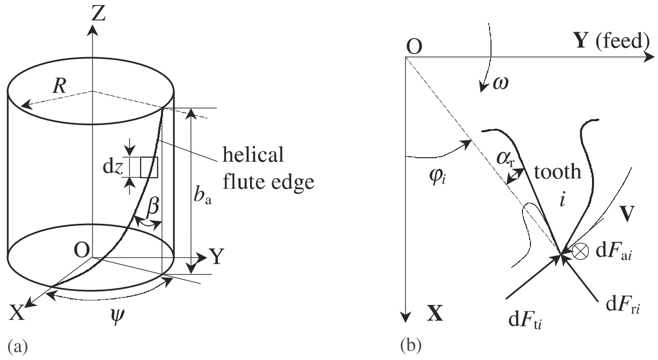

Fig. 1a,b. A diagrammatic illustration of the differential cutting force model of peripheral milling. **a** Helical flute geometry **b** Differential cutting forces

$$\mathrm{d}F_{\mathrm{t}i}(\varphi_i) = K_s t_i(\varphi_i) R \cot\beta \,\mathrm{d}\varphi \tag{1}$$

$$\mathrm{d}F_{\mathrm{r}i}(\varphi_i) = c_1 \mathrm{d}F_{\mathrm{t}i}(\varphi_i) \tag{2}$$

$$\mathrm{d}F_{\mathrm{a}i}(\varphi_i) = c_2 \mathrm{d}F_{\mathrm{t}i}(\varphi_i) \tag{3}$$

where $t_i(\varphi_i)$ is the undeformed chip thickness of the cutting point on the ith helical flute at position angle φ_i, and

$$\varphi_i = \varphi - \omega t_{\mathrm{ime}} + (i-1)\frac{2\pi}{m} \quad (1 \le i \le m, 0 \le \varphi \le \psi) \tag{4}$$

where

$$\psi = \frac{b_\mathrm{a} \tan\beta}{R} \tag{5}$$

is the axial immersion angle of a tooth within the axial depth of cut b_a.

In the model, K_s is the tangential cutting force coefficient, the radial force ratio c_1 varies depending on the cutter material and geometry, work material, and cutting conditions [12], and the axial force ratio can be determined using [13]

$$c_2 = \frac{\sin\beta(1-\sin\alpha_\mathrm{n}) - c_1 \cos\alpha_\mathrm{n} \tan\beta}{\sin\beta \sin\alpha_\mathrm{n} \tan\beta + \cos\beta} \tag{6}$$

where α_n is the normal rake angle of the helical flute [1].

According to the milling kinematics, and considering the influence of the cutter run-out, the undeformed chip thickness removed by the cutting point on the ith helical flute can be calculated as follows:

1. For down milling, as shown in Figure 2a:

$$t_i(\varphi_i') = \begin{cases} f_\mathrm{t} \sin(\varphi_i') + \delta t_i(\varphi_i') \mathrm{if} 0 \le \varphi_i' \le \Omega \\ 0 \mathrm{else} \end{cases} \tag{7}$$

2. For up milling, as shown in Figure 2b:

$$t_i(\varphi_i') = \begin{cases} f_\mathrm{t} \sin(-\varphi_i') + \delta t_i(\varphi_i') \mathrm{if} -\Omega \le \varphi_i' \le 0 \\ 0 \end{cases} \tag{8}$$

where $\delta t_i(\varphi_i')$ is the contribution of the cutter run-out to the undeformed chip thickness, which is given by:

$$\delta t_i(\varphi_i') \approx R_i'(\varphi_i') - R_{i-1}'(\varphi_i') \tag{9}$$

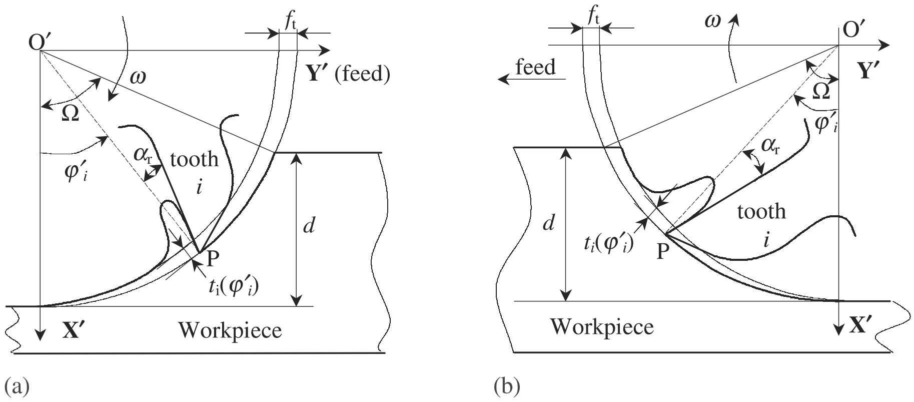

Fig. 2a,b. Peripheral milling. **a** Down milling **b** Up milling

where $R'_i(\varphi'_i)$ and $R'_{i-1}(\varphi'_i)$ are the actual cutting radius of the ith and the preceding tooth respectively, and

$$R'_i(\varphi'_i) = \sqrt{R^2 + \delta_e^2 - 2R\delta_e \cos(\angle \mathrm{O'OP})} \tag{10}$$

$$\angle \mathrm{O'OP} = \pi - |\varphi_i - \varphi_e| \tag{11}$$

where $\delta_e = \overline{OO'}$ is the cutter run-out value. O' is the spindle centre, and O is the cutter centre, as shown in Fig. 3.

In the initial position, the spindle rotational angle $\theta = -\omega t_{\mathrm{ime}} = 0$, let the initial location angle of the cutter centre be φ_{e0} $(0 \le \varphi_{e0} \le 2\pi)$. Assuming the initial location angle of the first tooth $(m = 1,\ \varphi = 0)$ is 0, so for the ith tooth of the cutter, when the helix lag angle $\varphi \neq 0$ and the spindle rotational angle $\theta \neq 0$, the location angle of the cutter centre

$$\varphi_e = \varphi_{e0} + \theta. \tag{12}$$

So by using Eq. 4, we can rewrite Eq. 10 as

$$R'_i(\varphi'_i) = \sqrt{R^2 + \delta_e^2 - 2R\delta_e \cos(\pi - |\varphi - \varphi_{e0} + 2(i-1)\pi/m|)}. \tag{13}$$

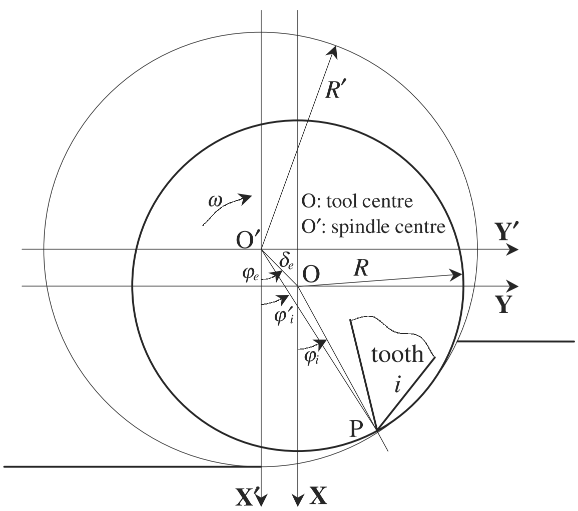

Fig. 3. The cutter run-out model

Resolving the differential cutting forces of Eqs. 1–Eq. 3 into the X, Y and Z directions yields (because $\delta_e \prec R$, so $\varphi'_i \approx \varphi_i$, $R'_i(\varphi'_i)\cot\beta \approx R\cot\beta$):

$$\begin{cases} \mathrm{d}F_{tix} = -K_s t_i(\varphi_i) R \cot\beta \sin\varphi_i \mathrm{d}\varphi \\ \mathrm{d}F_{tiy} = K_s t_i(\varphi_i) R \cot\beta \cos\varphi_i \mathrm{d}\varphi \end{cases} \tag{14}$$

$$\begin{cases} \mathrm{d}F_{rix} = -c_1 K_s t_i(\varphi_i) R \cot\beta \cos\varphi_i \mathrm{d}\varphi \\ \mathrm{d}F_{riy} = -c_1 K_s t_i(\varphi_i) R \cot\beta \sin\varphi_i \mathrm{d}\varphi \end{cases} \tag{15}$$

$$\mathrm{d}F_{iz} = -c_2 K_s t_i(\varphi_i) R \cot\beta \,\mathrm{d}\varphi \tag{16}$$

Summing these equations gives the differential forces in the X, Y and Z directions:

$$\begin{cases} \mathrm{d}F_{ix} = -K_s t_i(\varphi_i) R \cot\beta(\sin\varphi_i + c_1 \cos\varphi_i)\mathrm{d}\varphi \\ \mathrm{d}F_{iy} = K_s t_i(\varphi_i) R \cot\beta(\cos\varphi_i - c_1 \sin\varphi_i)\mathrm{d}\varphi \\ \mathrm{d}F_{iz} = -c_2 K_s t_i(\varphi_i) R \cot\beta \mathrm{d}\varphi \end{cases} \tag{17}$$

Considering the size effect of undeformed chip thickness and the influence of effective rake angle, gives the tangential cutting force coefficient K_s [1]

$$K_s = u_0 \left(1 - \frac{\alpha_e - \alpha_{e0}}{100}\right) \left(\frac{t_0}{t_i(\varphi_i)}\right)^{0.2}. \tag{18}$$

Letting

$$u' = u_0 \left(1 - \frac{\alpha_e - \alpha_{e0}}{100}\right) \left(\frac{t_0}{f_t}\right)^{0.2}, \tag{19}$$

the tangential cutting force coefficient can be approximated by (assuming $\delta t_i(\varphi_i) \prec t_i(\varphi_i)$):

1. For down milling:

$$K_s \approx u'(\sin\varphi_i)^{-0.2}(0 \le \varphi_i \le \Omega) \tag{20}$$

2. For up milling:

$$K_s \approx u'[\sin(-\varphi_i)]^{-0.2}(-\Omega \le \varphi_i \le 0) \tag{21}$$

By applying Eqs. 20 and 21, and noting that $\mathrm{d}\varphi_i = \mathrm{d}\varphi$, Eq. 17 becomes:

1. For down milling:

$$\begin{cases} \mathrm{d}F_{ix} = -u'(f_t \sin(\varphi_i) \\ \qquad +\delta t_i(\varphi_i'))R\cot\beta(\sin^{0.8}\varphi_i + c_1\sin^{-0.2}\varphi_i\cos\varphi_i)\mathrm{d}\varphi_i \\ \mathrm{d}F_{iy} = u'(f_t\sin(\varphi_i) \\ \qquad +\delta t_i(\varphi_i'))R\cot\beta(\sin^{-0.2}\varphi_i\cos\varphi_i - c_1\sin^{0.8}\varphi_i)\mathrm{d}\varphi_i \\ \mathrm{d}F_{iz} = -u'(f_t\sin(\varphi_i) \\ \qquad +\delta t_i(\varphi_i'))R\cot\beta(c_2\sin^{-0.2}\varphi_i)\mathrm{d}\varphi_i \end{cases} \tag{22}$$

$$\begin{pmatrix} \varphi_i = \varphi - \omega t_{\mathrm{ime}} + (i-1)\frac{2\pi}{m} \\ 0 \le \varphi_i \le \Omega \end{pmatrix}$$

2. For up milling:

$$\begin{cases} \mathrm{d}F_{ix} = -u'(f_t\sin(-\varphi_i) + \delta t_i(\varphi_i'))R\cot\beta \\ \qquad \times\left[-\sin^{0.8}(-\varphi_i) + c_1\sin^{-0.2}(-\varphi_i)\cos\varphi_i\right]\mathrm{d}\varphi_i \\ \mathrm{d}F_{iy} = u'(f_t\sin(-\varphi_i) + \delta t_i(\varphi_i'))R\cot\beta \\ \qquad \times\left[\sin^{-0.2}(-\varphi_i)\cos\varphi_i + c_1\sin^{0.8}(-\varphi_i)\right]\mathrm{d}\varphi_i \\ \mathrm{d}F_{iz} = -u'(f_t\sin(-\varphi_i) + \delta t_i(\varphi_i'))R\cot\beta \\ \qquad \times\left[c_2\sin^{-0.2}(-\varphi_i)\right]\mathrm{d}\varphi_i \end{cases} \tag{23}$$

$$\begin{pmatrix} \varphi_i = \varphi - \omega t_{\mathrm{ime}} + (i-1)\frac{2\pi}{m} \\ -\Omega \le \varphi_i \le 0 \end{pmatrix}$$

where $(1 \le i \le m, 0 \le \varphi \le \psi)$.

The total cutting force applied on the whole cutting edge is given by

$$\begin{cases} F_{ix} = \int_{\varphi_s}^{\varphi_e} \mathrm{d}F_{ix}\mathrm{d}\varphi_i \\ F_{iy} = \int_{\varphi_s}^{\varphi_e} \mathrm{d}F_{iy}\mathrm{d}\varphi_i \\ F_{iz} = \int_{\varphi_s}^{\varphi_e} \mathrm{d}F_{iz}\mathrm{d}\varphi_i \end{cases} \tag{24}$$

where φ_s and φ_e are the lag angular locations of the start and end points of contact of the cutting edge, and are defined in the following kinematics analysis.

1. For down milling: Because $0 \le \varphi \le \psi$, $\varphi_i = \varphi - \omega t_{\mathrm{ime}} + (i-1)\frac{2\pi}{m}$ and $0 \le \varphi_i \le \Omega$ give the extreme values of the parametric angle φ_i as:

$$\varphi_s = \max(0, -\omega t_{\mathrm{ime}} + (i-1)\frac{2\pi}{m}) \tag{25}$$

$$\varphi_e = \min(\Omega, \psi - \omega t_{\mathrm{ime}} + (i-1)\frac{2\pi}{m}) \tag{26}$$

2. For up milling: Also, $0 \le \varphi \le \psi$, $\varphi_i = \varphi - \omega t_{\mathrm{ime}} + (i-1)\frac{2\pi}{m}$ and $-\Omega \le \varphi_i \le 0$ give the extreme values of the parametric angle φ_i as:

$$\varphi_s = \max(-\Omega, -\omega t_{\mathrm{ime}} + (i-1)\frac{2\pi}{m}) \tag{27}$$

$$\varphi_e = \min(0, \psi - \omega t_{\mathrm{ime}} + (i-1)\frac{2\pi}{m}) \tag{28}$$

Summing up the cutting forces acting on all the m helical flutes gives the total force applied on the whole cutter.

$$\begin{cases} F_x = \sum_{i=1}^{m} F_{ix} \\ F_y = \sum_{i=1}^{m} F_{iy} \\ F_z = \sum_{i=1}^{m} F_{iz} \end{cases} \tag{29}$$

3 Experimental calibration of cutting force coefficients

In the cutting force model, the following three coefficients are to be calibrated by experiment:

1. u_0, the initial total cutting energy per unit volume, under the initial cutting condition $\alpha_{e0} = 0°$ and $t_0 = 0.25$ mm [12]
2. c_1, the radial force ratio
3. c_2, the axial force ratio

The value of u_0 depends on the workpiece material, cutter material, cutting edge radius, friction characteristics between the workpiece and the cutter (no built-up edge is assumed), whereas the ratios c_1 and c_2 rely mainly on the cutter geometry. Although c_2 can be obtained from c_1 and cutter geometry using Eq. 6 [13], it needs to be calibrated by experiments, due to the inconsistency between the calculated value and the experimental data.

In order to avoid the interference of the cutting force generated by adjacent teeth, a one-tooth helical end mill is used in the cutting trials for the calibration of cutting force coefficients. It can be seen from Eq. 9 that a small cutter run-out (no matter how much the value and its initial location angle φ_{e0} are) theoretically has no influence on the cutting force. In order to obtain a maximum radial immersion angle, a set of slot milling tests were carried out with the cutting conditions and parameters as listed in Table 1.

The experimental work was performed on a three axis vertical CNC machine centre, Cincinnati Arrow2-500. The 3D dynamic cutting forces were recorded by the Kistler table dy-

Table 1. Cutting conditions and parameters (slot milling)

Cutter: a single fluted solid carbide end-mill, $R = 10$ mm, $\beta = 45°$, $\alpha_r = 5°$
Work material: carbon steel EN8
Cutting condition: with fluid
Cutting parameters: spindle rotation speed $n = 1114$ rpm (cutting speed $v = 70$ m/min), feed rate f_t in mm/tooth, axial depth of cut b_a in mm

$f_t = 0.0197$	$b_a = 10.545$
$f_t = 0.0296$	$b_a = 10.545$
$f_t = 0.0395$	$b_a = 10.545$
$f_t = 0.0494$	$b_a = 10.45$
$f_t = 0.0592$	$b_a = 10.39$
$f_t = 0.0691$	$b_a = 10.45$
$f_t = 0.0790$	$b_a = 10.39$
$f_t = 0.0889$	$b_a = 10.39$

namometer, 9257BA, and mounted on the worktable of the machine tool. Machine vibrations were monitored using piezoelectric accelerometers mounted on the spindle head, and workpiece vibrations were examined by the accelerometers mounted on the workpiece itself, which was fixed using the Microloc fixture system, Kit-75, mounted on the dynamometer. Figure 4 illustrates the experimental configuration and setup.

For estimating the cutting force coefficients, the easiest and probably best way is to use the average cutting forces. The theoretical average cutting force components can be asserted from Eqs. 22 to 29 as

$$\begin{cases} \bar{F}_x = u_0 \sum\limits_{i=1}^{m} \bar{f}_{ix1} + u_0 c_1 \sum\limits_{i=1}^{m} \bar{f}_{ix2} \\ \bar{F}_y = u_0 \sum\limits_{i=1}^{m} \bar{f}_{iy1} + u_0 c_1 \sum\limits_{i=1}^{m} \bar{f}_{iy2} \\ \bar{F}_z = u_0 c_2 \sum\limits_{i=1}^{m} \bar{f}_{iz} \end{cases} \tag{30}$$

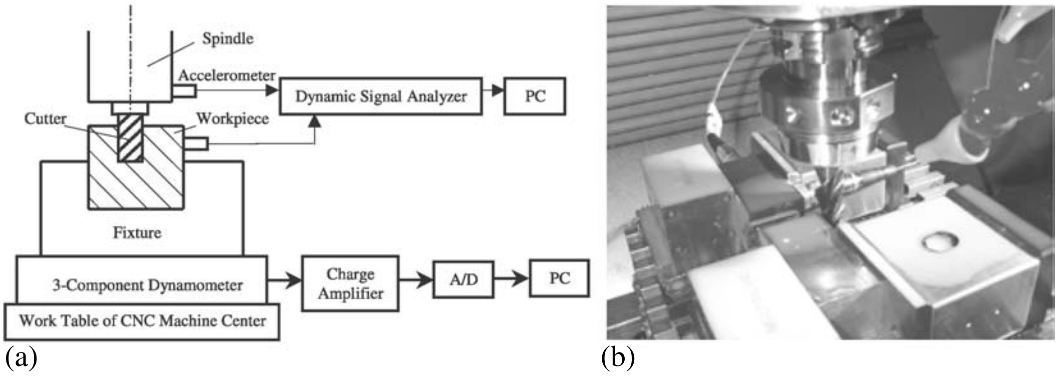

Fig. 4. Experimental configuration of cutting tests

Table 2. Experimentally calibrated cutting force coefficients (by slot milling)

f_t(mm/tooth)	0.0197	0.0296	0.0395	0.0494	0.0592	0.0691	0.0790	0.0889
u_0(G J/m^3)	2.4067	2.4433	2.3851	2.4532	2.3891	2.5146	2.4429	2.5184
c_1	0.5114	0.4832	0.4776	0.3889	0.3457	0.4052	0.3992	0.4171
c_2	0.2617	0.2871	0.3191	0.3529	0.3525	0.3596	0.3570	0.3599
Calculated c_2	0.2038	0.2413	0.2448	0.3667	0.4241	0.3540	0.3530	0.3292

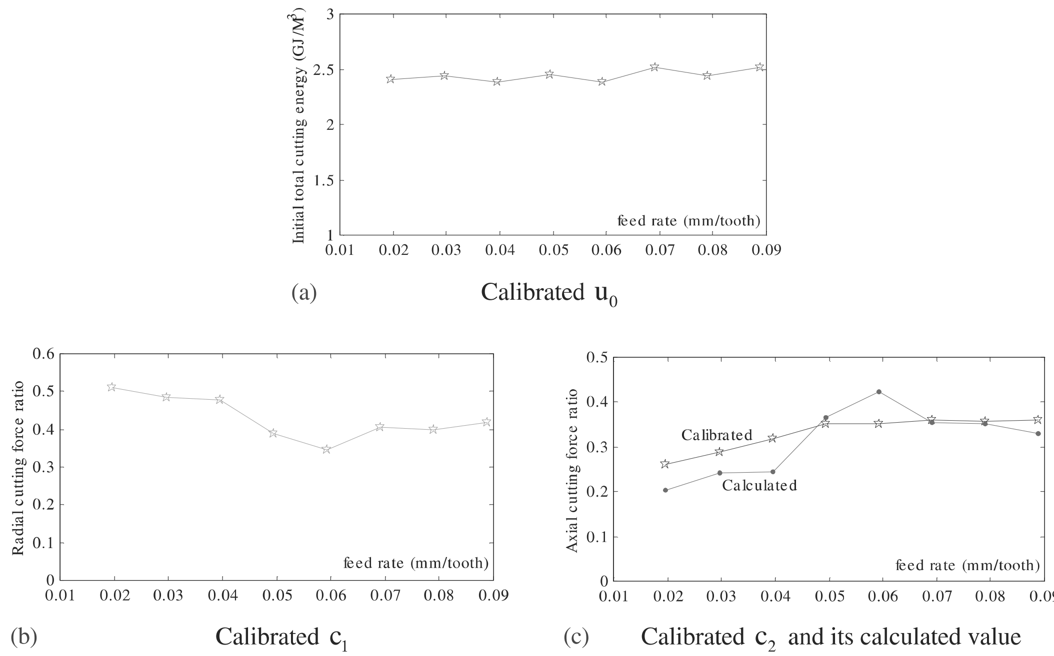

Fig. 5. Experimentally calibrated cutting force coeficients (by slot milling)

where

1. For down milling:

$$f_{ix1} = \int_{\varphi_s}^{\varphi_e} -c_s \sin^{0.8} \varphi_i \mathrm{d}\varphi_i$$

$$f_{ix2} = \int_{\varphi_s}^{\varphi_e} -c_s \sin^{-0.2} \varphi_i \cos\varphi_i \mathrm{d}\varphi_i$$

$$f_{iy1} = \int_{\varphi_s}^{\varphi_e} c_s \sin^{-0.2} \varphi_i \cos\varphi_i \mathrm{d}\varphi_i$$

Fig. 6. Measured and predicted cutting forces in slot milling

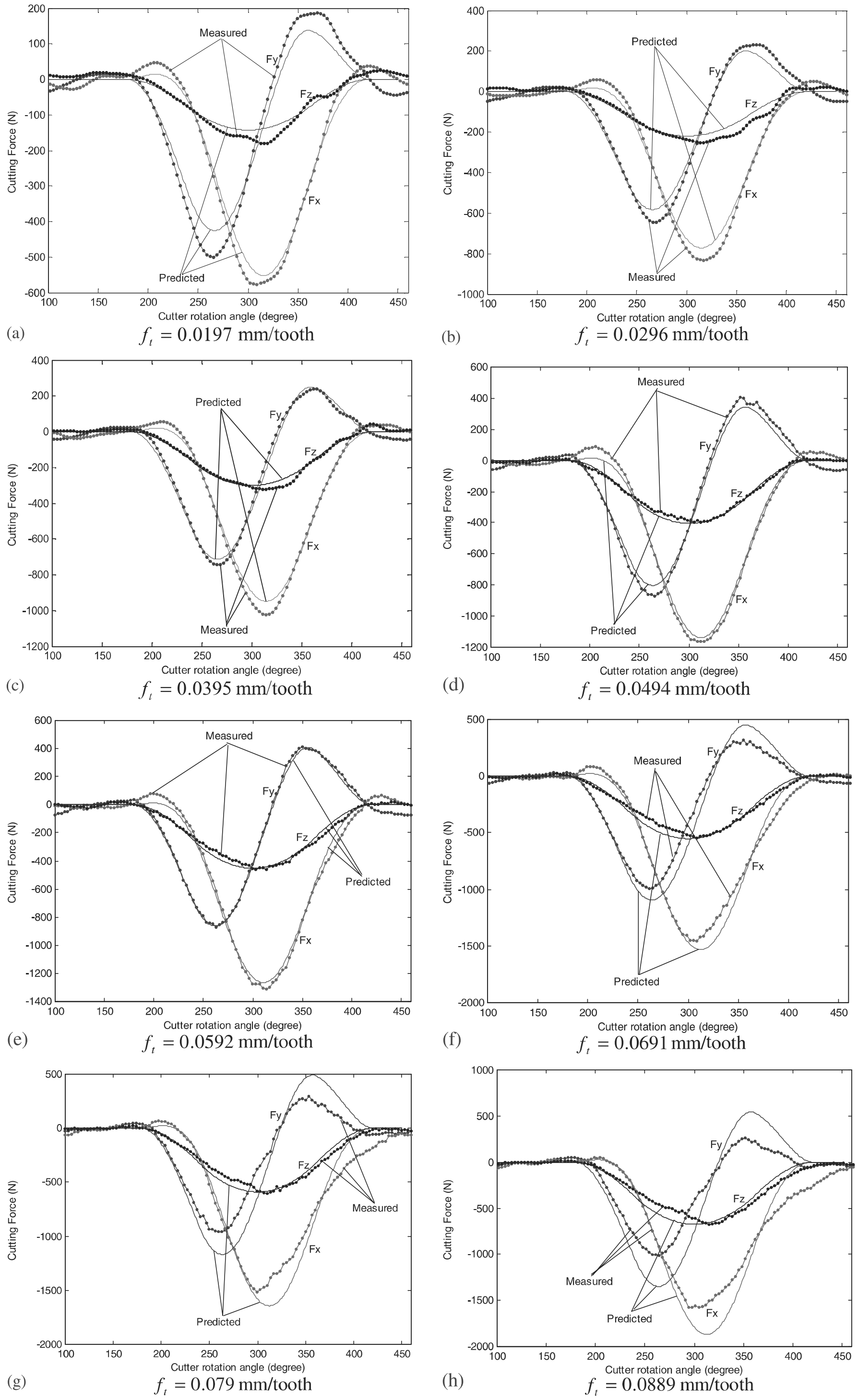

$$f_{iy2} = \int_{\varphi_s}^{\varphi_e} -c_s \sin^{0.8} \varphi_i \mathrm{d}\varphi_i$$

$$f_{iz} = \int_{\varphi_s}^{\varphi_e} -c_s \sin^{-0.2} \varphi_i \mathrm{d}\varphi_i$$

$$c_s = \left(1 - \frac{\alpha_e - \alpha_{e0}}{100}\right)\left(\frac{t_0}{f_t}\right)^{0.2} \left(f_t \sin(\varphi_i) + \delta t_i(\varphi_i')\right) R \cot \beta \tag{31}$$

2. For up milling:

$$f_{ix1} = \int_{\varphi_s}^{\varphi_e} c_s \sin^{0.8}(-\varphi_i) \mathrm{d}\varphi_i$$

$$f_{ix2} = \int_{\varphi_s}^{\varphi_e} -c_s \sin^{-0.2}(-\varphi_i) \cos\varphi_i \mathrm{d}\varphi_i$$

$$f_{iy1} = \int_{\varphi_s}^{\varphi_e} c_s \sin^{-0.2}(-\varphi_i) \cos\varphi_i \mathrm{d}\varphi_i$$

$$f_{iy2} = \int_{\varphi_s}^{\varphi_e} c_s \sin^{0.8}(-\varphi_i) \mathrm{d}\varphi_i$$

$$f_{iz} = \int_{\varphi_s}^{\varphi_e} -c_s \sin^{-0.2}(-\varphi_i) \mathrm{d}\varphi_i$$

$$c_s = \left(1 - \frac{\alpha_e - \alpha_{e0}}{100}\right)\left(\frac{t_0}{f_t}\right)^{0.2} \left(f_t \sin(-\varphi_i) + \delta t_i(\varphi_i')\right) R \cot \beta \tag{32}$$

Averaging the cutting forces from the measured dynamic forces and substituting them into Eq. 30 can yield the cutting force coefficients u_0, c_1 and c_2. Table 2 and Fig. 5 show the calibrated cutting force coefficients, in which u_0 varies between 2.3851×10^9 and $2.5184 \times 10^9 \mathrm{J/m^3}$, c_1 between 0.3457 and 0.5114, and c_2 between 0.2617 and 0.3599.

It is worth mentioning that using Eq. 6 with the calibrated c_1 gives the calculated c_2, as illustrated in Fig. 5c. There is a small difference between the experimental calibration and the estimated evaluation for the axial force ratio c_2.

Figure 6 shows the measured and predicted dynamic cutting force components in the directions X, Y and Z, in which the predicted ones are generated based on the proposed cutting force model with the calibrated force coefficients.

The results shown in Fig. 6 reveal that there is a good agreement between the measured and predicted cutting forces when the feed rate changes from $f_t = 0.0395$mm/tooth to $f_t =$

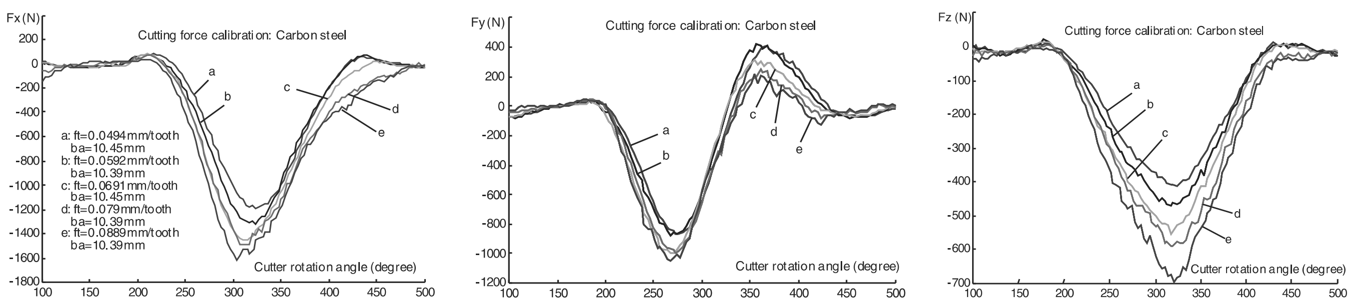

Fig. 7. Measured cutting forces in slot milling

Table 3. Cutting conditions and parameters (peripheral milling)

Cutter: solid carbide end-mill, $R = 10$ mm, $\alpha_r = 5°$
Work material: carbon steel EN8
Cutting condition: with fluid

Test no.	Tooth no.	Helix angle	δ_e (mm)*	Spindle rotation speed (rpm)	SF (Hz)	TPF (Hz)	Feed rate (mm/tooth)	Axial depth of cut (mm)	Radial depth of cut (mm)
1	$m = 2$	30°	0.002	$n = 1592$	26.5333	53.0667	$f_t = 0.05$	$b_a = 5.105$	$d = 10.8$
2	$m = 3$	30°	0.003	$n = 1114$	18.5667	55.7	$f_t = 0.06$	$b_a = 15.03$	$d = 2.021$
3	$m = 3$	30°	0.005	$n = 1751$	29.1833	87.55	$f_t = 0.05$	$b_a = 5.107$	$d = 10.83$
4	$m = 8$	45°	0.003	$n = 1592$	26.5333	212.2667	$f_t = 0.05$	$b_a = 15.05$	$d = 2.022$

SF: Spindle frequency, TPF: Tooth passing frequency
*The cutter run-out was measured using a non-contact displacement transducer

0.0592mm/tooth. When the feed rate $f_t < 0.0395$mm/tooth, the measured cutting force components F_x and F_y are greater than the predicted ones. That means the calibrated u_0 is smaller than its actual value. When the feed rate $f_t > 0.0592$mm/tooth, the measured cutting force components F_x and F_y are smaller than the predicted ones. That means the calibrated u_0 is greater than its actual value. Putting the measured cutting forces together, as shown in Fig. 7, reveals that our experimental result differs from the experimental results published [8]. This result indicates the size effect of undeformed chip thickness and the influence of the effective rake angle may be more significant than the estimated value from Eq. 19. Meanwhile it also reveals that the proposed model is valid only when feed rate changes from $f_t = 0.0395$mm/tooth to $f_t = 0.0592$mm/tooth.

4 Experimental verification

A series of peripheral milling tests on the carbon steel were undertaken with different helical end mills and different cutting parameters. Table 3 lists the cutting conditions and parameters of these tests, and Figs. 8–11 compare the measured and predicted dynamic cutting forces, in which the predicted values are obtained from the cutting force model using the evaluated cutting force coefficients by averaging the cutting forces from the measured dynamic ones and substituting them into Eq. 30.

Figure 8 shows the measured and predicted cutting forces, and the measured power spectra of the first test. The influence of the

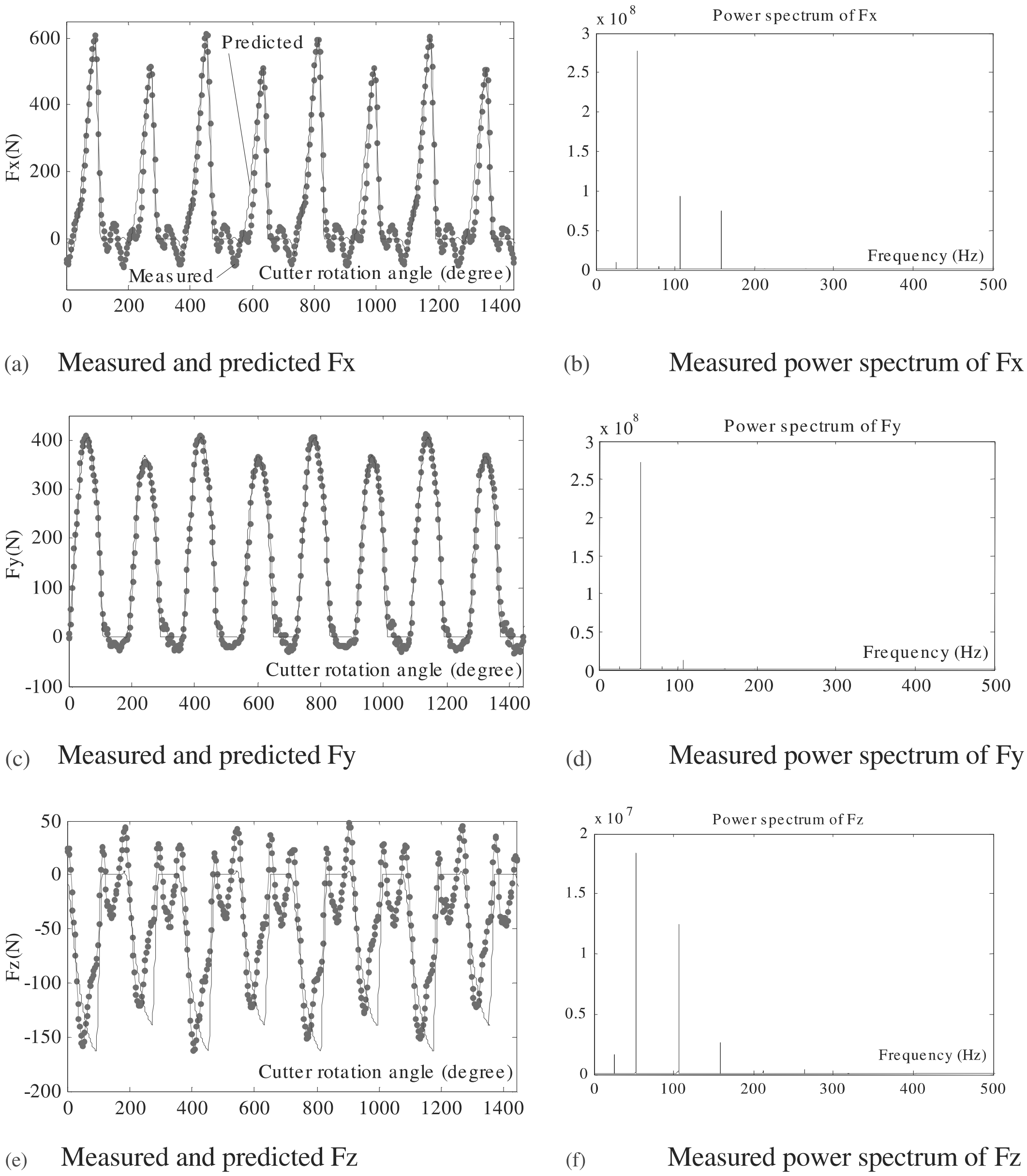

(a) Measured and predicted Fx
(b) Measured power spectrum of Fx
(c) Measured and predicted Fy
(d) Measured power spectrum of Fy
(e) Measured and predicted Fz
(f) Measured power spectrum of Fz

Fig. 8. Measured and predicted cutting forces for peripheral milling (Test No. 1)

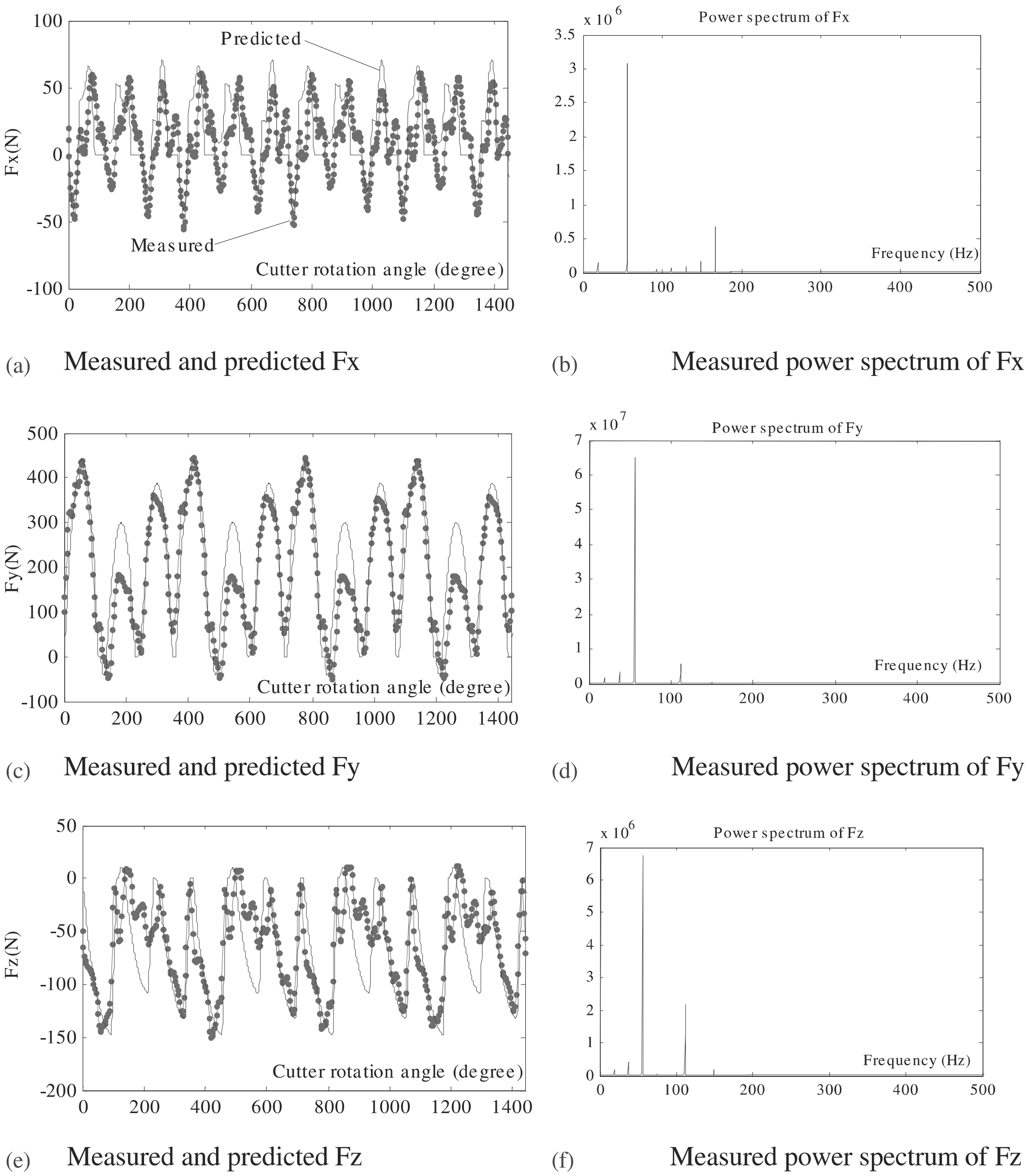

Fig. 9. Measured and predicted cutting forces for peripheral milling (Test No. 2)

cutter run-out on the cutting forces is obvious, and there is a measure of vibrations in the X and Z directions at the frequencies 2TPF and 3TPF, and this is the main reason for the inconsistency between the measured and predicted cutting forces. The evaluated main cutting force coefficient $u_0 = 1.8064 \times 10^9$ J/m^3, which is obviously smaller than the calibrated u_0 (2.4532×10^9 J/m^3), this is because the spindle speed increases from 1114rpm to 1592rpm. The result confirms that the measured and predicted cutting forces in the X and Y directions have a reasonable agreement when the vibrations at the frequencies of times TPF are faint.

It is worth mentioning that the predicted cutting forces depend on the initial location angle of the cutter centre φ_{e0}.

Figure 9 records the measured and predicted cutting forces, and the measured power spectra of the second test. The result reveals that the cutter run-out also has obvious influence on the cutting forces, there is a measure of vibrations at the frequency 3TPF in the X direction and at 2TPF in the Z direction, and the actual cutter run-out value seems greater than the measured value because of the inconsistency between the measured and predicted cutting forces.

Figure 10 illustrates the measured and predicted cutting forces, and the measured power spectra of the third test. The power spectra of the measured cutting forces reveal that the influence of the cutter run-out on the cutting forces is dominant, even though its value ($\delta_e = 0.005$mm) is far smaller than the feed rate ($f_t = 0.05$mm/tooth). There is also a considerable vibration in the cutting process, especially in the Z direction, and this is the main reason for the inconsistency between the meas-

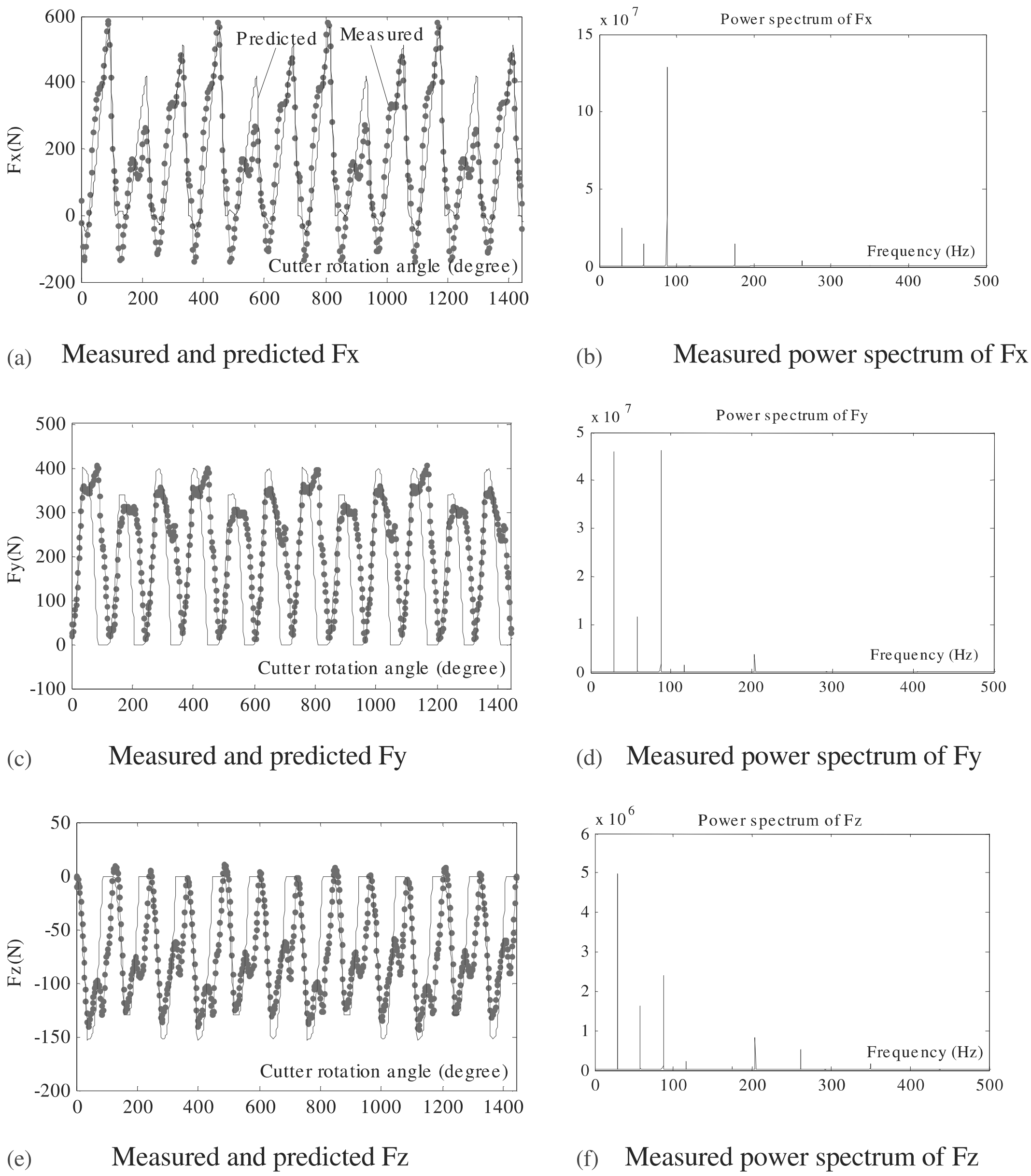

Fig. 10. Measured and predicted cutting forces for peripheral milling (Test No. 3)

ured and predicted cutting forces. The cutting force coefficient $u_0 = 1.7543 \times 10^9$, evaluated from the measured cutting forces, is smaller than the calibrated value, this is because the spindle speed increases from 1114 rpm to 1751 rpm. The result also indicates that the measured and predicted cutting forces are in reasonable agreement.

Figure 11 presents the measured and predicted cutting forces, and the measured power spectra of the fourth test. The result indicates that the influence of the cutter run-out on the cutting forces is dominant: the peak values of the FFT of the measured cutting forces at the SF are far greater than that at the TPF. The main reason of this influence is the increased tooth number ($m = 8$) of the cutter. From the measured cutting forces and their power spectra, we can not discern any serious vibration in the cutting process. However, as a matter of fact, chatter occurs in the cutting process at a frequency of 776.5Hz, which is recorded by accelerometers. This is the main reason for the inconsistency of the amplitudes between the measured and predicted cutting forces at the TPF.

In a general case, the main cutting force component at the TPF excites a dominant vibration (forced vibration) of the cutting system, which in turn influences the dynamic cutting forces. When the displacement amplitude of the vibration is well controlled, its influence on the dynamic cutting forces will be undistinguished. This is proven by the results shown in Fig. 8. When the vibration is severe, there is a distinguished inconsistency between the predicted and measured dynamic cutting forces, as shown in Figs. 9, 10 and 11.

Fig. 11. Measured and predicted cutting forces for peripheral milling (Test No. 4)

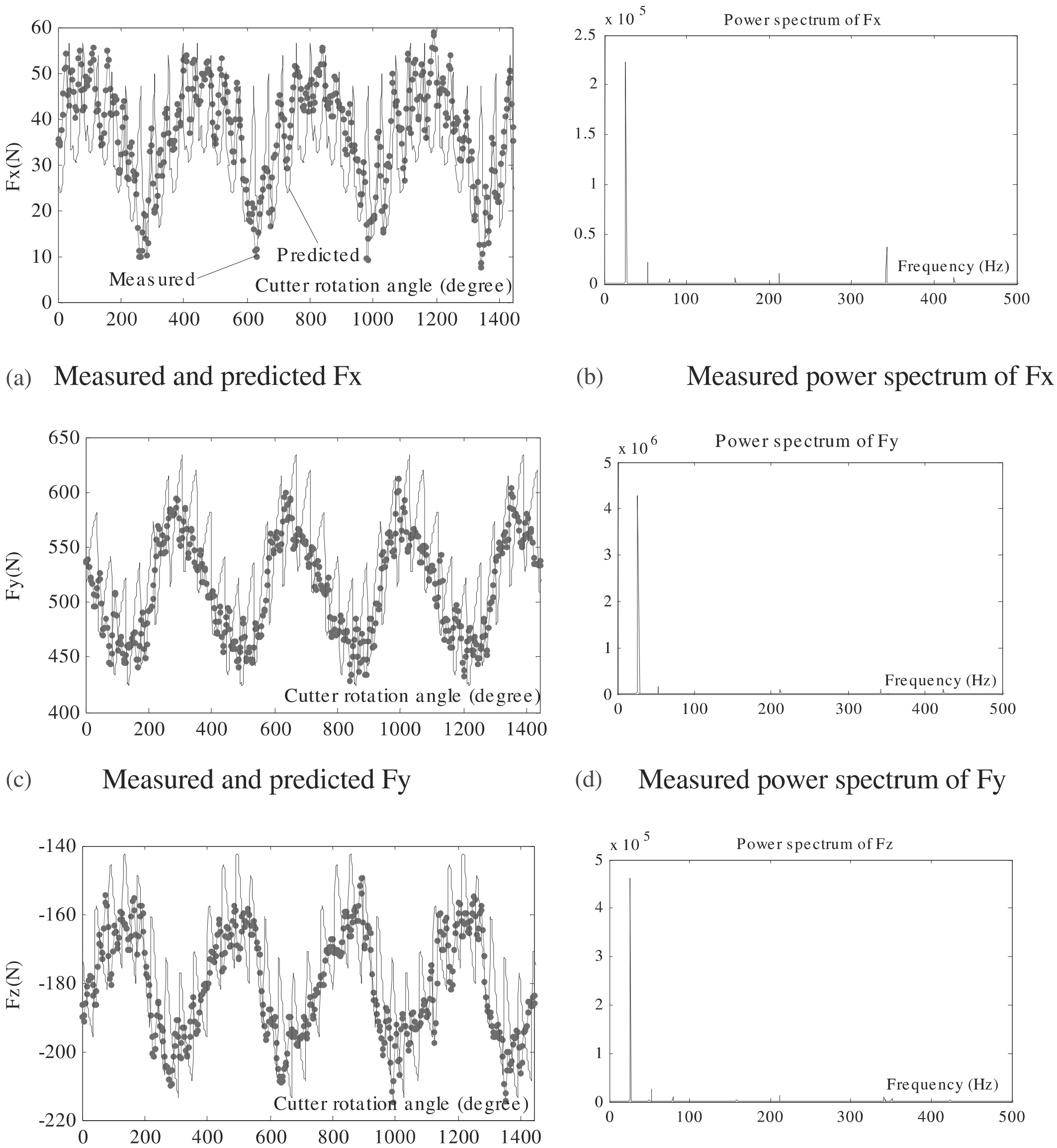

(a) Measured and predicted Fx (b) Measured power spectrum of Fx

(c) Measured and predicted Fy (d) Measured power spectrum of Fy

(e) Measured and predicted Fz (f) Measured power spectrum of Fz

5 Discussion and conclusions

The cutting test results indicate that a measure of cutter run-out is always unavoidable. Based on this fact and a theoretical analytical model [1], this paper proposes to improve the dynamic cutting force model in peripheral milling, which takes into account the influence of the cutter run-out on the undeformed chip thickness.

The results of experimental calibration of the cutting force coefficients show that the theoretical evaluation for the axial force ratio c_2 based on Eq. 6 [13] is not precise enough and must be calibrated by experiment. Using the improved model with the calibrated cutting force coefficients, the predicted and measured cutting forces in slotting with a single fluted end mill are in reasonable agreement.

The results of cutting tests for the verification of the model reveal that the vibrations between the cutter and workpiece are unavoidable. In spite of the force component at the tooth passing frequency, other components, i.e., at the times TPF, the spindle frequency (corresponding to the cutter run-out) and its times frequencies, might excite vibrations between the cutter and workpiece. Only when the vibration is faint, using the improved model with the calibrated cutting force coefficients, the predicted and measured cutting forces in peripheral milling have a good agreement. When a distinguished vibration or chatter is excited during the cutting process, there will be a significant difference between the predicted and measured cutting forces. A more precise dynamic cutting force model must include the vibrations between the cutter and workpiece and be integrated into a machining dynamics model.

The experimental results reveal that the cutting force coefficient u_0 decreases when the cutting speed increases. A comprehensive machining dynamics model must take account of the influence of the cutting parameters on the cutting forces.

Acknowledgement The authors would like to give thanks to the EPSRC for grant support (EPSRC GR/R13395) and also to the collaborating partners, Cincinnati (UK) Ltd, Kistler Ltd, Renishaw plc, Siemens (UK) Ltd and Widia GmbH (Germany), for their financial support, advice and practical assistance.

References

1. Liu X-W, Cheng K, Webb D (2002) Improved dynamic cutting force model in peripheral milling. Part I: Theoretical model and simulation. Int J Adv Manuf Technol 20(9):631–638
2. Bayoumi AE, Yucesan G, Kendall LA (1994) An analytic mechanistic cutting force model for milling operations: a theory and methodology. Trans ASME J Eng Ind 116:324–339
3. Budak E, Altintas Y, Armarego EJA (1996) Prediction of milling force coefficients from orthogonal cutting data. Trans ASME J Manuf Sci Eng 118(2):216–224
4. Kolarits FM, DeVries WR (1991) A mechanistic dynamic model of end milling for process controller simiulation. Trans ASME J Eng Ind 113:176–183
5. Elbestawi MA, Ismail F, Du R, Ullagaddi BC (1994) Modelling machining dynamics including damping in the tool-workpiece interface. Trans ASME J Eng Ind 116:435–439
6. Ismail F, Elbestawi MA, Du R, Urbasik K (1993) Generation of milled surface including tool dynamics and wear. Trans ASME J Eng Ind 115:245–252
7. Montgomery D, Altintas Y (1991) Mechanism of cutting force and surface generation in dynamic milling. Trans ASME J Eng Ind 113:160–168
8. Yucesan GB, Altintas Y (1994) Improved modelling of cutting force coefficients in peripheral milling. Int J Mach Tools Manuf 34(4):473–487
9. Smith S, Tlusty J (1991) An overview of modeling and simulation of the milling process. Trans ASME J Eng Ind 113:169–175
10. Melkote SN, Endres WJ (1998) The importance of including size effect when modeling slot milling. Trans ASME J Manuf Sci Eng 120:68–75
11. Yun W-S, Cho D-W (2000) An improved method for the determination of 3D cutting force coefficients and runout parameters in end milling. Int J Adv Manuf Technol 16:851–858
12. Shaw MC (1984) Metal cutting principles. Oxford University Press, Oxford
13. Oxley PLB (1989) The mechanics of machining. Ellis Horwood, Chichester